

# Bursting dynamics in a population of oscillatory and excitable Josephson junctions

Chittaranjan Hens,<sup>1,2</sup> Pinaki Pal,<sup>3</sup> and Syamal K. Dana<sup>1</sup>

<sup>1</sup>*CSIR-Indian Institute of Chemical Biology, Kolkata 700032, India*

<sup>2</sup>*Department of Mathematics, Bar-Ilan University, Ramat Gan 52900, Israel*

<sup>3</sup>*Department of Mathematics, National Institute of Technology, Durgapur 713209, India*

(Received 27 February 2015; revised manuscript received 14 June 2015; published 20 August 2015)

We report an emergent bursting dynamics in a globally coupled network of mixed population of oscillatory and excitable Josephson junctions. The resistive-capacitive shunted junction (RCSJ) model of the superconducting device is considered for this study. We focus on the parameter regime of the junction where its dynamics is governed by the saddle-node on invariant circle (SNIC) bifurcation. For a coupling value above a threshold, the network splits into two clusters when a reductionism approach is applied to reproduce the bursting behavior of the large network. The excitable junctions effectively induce a slow dynamics on the oscillatory units to generate parabolic bursting in a broad parameter space. We reproduce the bursting dynamics in a mixed population of dynamical nodes of the Morris-Lecar model.

DOI: [10.1103/PhysRevE.92.022915](https://doi.org/10.1103/PhysRevE.92.022915)

PACS number(s): 05.45.Xt, 05.45.Gg, 85.25.Cp, 87.19.lm

## I. INTRODUCTION

The superconducting Josephson junction shows self-oscillation [1–3] for an applied constant current above a critical value. It is usually modeled as a resistive-capacitive-shunted junction (RCSJ) which has its mechanical analog in a damped pendulum with a constant torque. A RCL-shunted junction (resistive-capacitive inductively shunted junction) model [4–8] was also used to include an inductive loading effect in an array of junctions where more complex dynamics including chaos was reported. Interestingly, the superconducting device shows spiking and bursting behaviors [9,10] most commonly seen in the Type I excitability neuron [11]. The bursting dynamics was found prominent [6,9,12] in a periodically forced junction. This is due to the intrinsic SNIC characteristic of the junction in a dominant parameter regime [3,9,13]. The SNIC bifurcation governs [11] a class of bursting dynamics in Type I excitability neurons.

Spiking is a repetitive firing state and bursting is a state of recurrent switching between a firing state or oscillatory state and a resting state. The minimal condition for bursting in a system necessitates the presence of an intrinsic slow-fast dynamics [11,14–16]. Alternatively, an excitable system when coupled to an oscillatory system was also found [17] to induce a slow dynamics and thereby originates a type of chaotic bursting.

We focus on the collective dynamics of a population of globally coupled RCSJs and are, particularly, interested in the parameter region of the junction where it behaves like the Type-I excitability neurons, excitable or oscillatory. Collective behaviors of coupled RCSJ arrays are an important issue of both device specific [18] and general interest [8,19], however, the issue of neuron-like excitability of coupled junctions was not considered earlier to the best of our knowledge. On a general context, the collective behavior of an ensemble of a mixed population of globally coupled passive or excitable and active or oscillatory units was investigated earlier [20–24] in search of a global oscillation. Such a global oscillation is practically important, particularly, in the context of a desired response of the pacemaker cells [25,26]. It is important to know, in the event of a growing cell death, how robust are

the pacemaker cells in the heart or the suprachiasmatic cells in the brain to sustain a global oscillation? In the dynamical sense, the death of a cell is considered there as a passive state or an excitable state. In a situation of progressive cell death, in other words, increasing number of passive oscillators, a population of globally coupled oscillators showed a type of aging transition [20]. In this aging transition, the whole population emerges into a quiescent state; besides this death regime, partial oscillation and global oscillation (1:1 and higher frequency ratios) persist [21] in regions of parameter space of the coupling strength and the number of excitable units. The global oscillation is desired for pacemaker cells to sustain their activity. However, the specific dynamical nature of the global oscillation was not given appropriate attention, which we emphasize here using a mixed population of the superconducting junction and further verify the nature of the dynamics using the Morris-Lecar model [21,27].

We construct a globally coupled network (Fig. 1) of mixed populations of excitable and oscillatory RCSJs. We select a particular but dominant parameter space of the junction where its dynamics is governed [1,3] by the SNIC bifurcation. In that parameter space, the RCSJ units are excitable when they are in a stable steady state for a bias current less than a critical value and become oscillatory via the SNIC bifurcation when the bias current is above the critical value. We observe that the presence of a fraction of excitable junctions generates a bursting in the whole network although the uncoupled oscillatory junctions never show bursting dynamics. The excitable units provide the necessary slow dynamics for the generation of bursting. For a coupling strength above a threshold, the mixed population of the network starts firing with a single spiking. For a further increase of coupling, one spike after another is added to form a periodic bursting and eventually the parabolic bursting emerges. During the spiking and bursting, the network splits into two clusters (Fig. 2), one forming a manifold of the excitable units, now oscillatory, and another of the original self-oscillatory units. Two almost similar burstings emerge from the two subpopulations which closely follow each other in time and are seen to be correlating although the individual spikes are not. At the start of the bursting, two clusters lag behind each other and after a few spikes they coincide in time

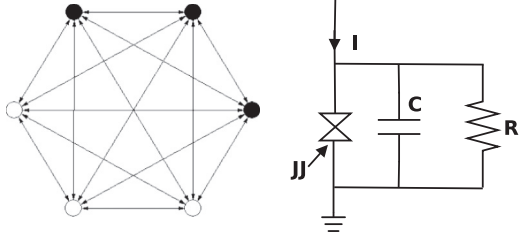


FIG. 1. Globally coupled network of size  $N = 6$  (left panel) with excitable (black circle) and oscillatory (open circle) nodes. A single Josephson junction is shown at right representing each node of the network. Each RCSJ is diffusively connected to the other via voltage variables at the resistor or capacitor node.

which is evident at the end of each burst and then start moving together towards the quiescent state and repeats the bursting after a recovery period. In the two-clustered state, we reduce the network model using two manifolds of the self-oscillatory and excitable units and numerically reproduce the bursting dynamics of the whole network.

We organize the text in the following manner. We describe the RCSJ model in the next section. The network model is described in Sec. III. The reduced model and the bursting mechanism is elaborated in Sec. IV. Results of a network using the Morris-Lecar model that also shows bursting dynamics is demonstrated in Sec. V. Results are summarized in Sec. VI.

## II. SINGLE JUNCTION MODEL

A single RCSJ model is described by

$$\ddot{\theta} + \alpha\dot{\theta} + \sin\theta = I, \quad (1)$$

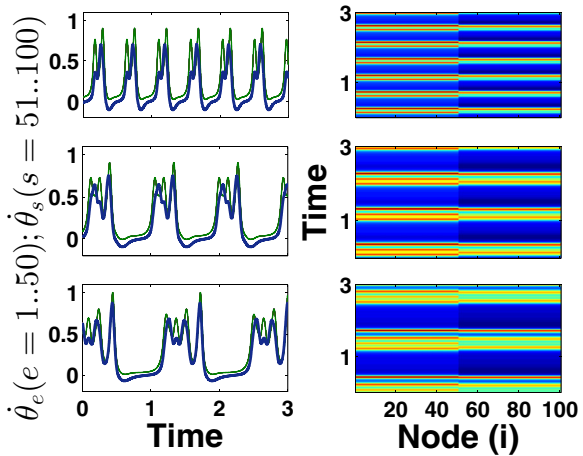


FIG. 2. (Color online) Bursting dynamics in a network of Josephson junctions. Two time series are seen (left panels), one represents all the excitable nodes ( $e = 1, \dots, 50$ ) merged into one (thick blue) and the other represents all the oscillatory nodes merging into another (green) ( $s = 51, \dots, 100$ ). Temporal dynamics of all the nodes are shown in the right panels for  $N = 1$  to  $100$ . Fraction of excitable units in the network,  $p = 0.5$  and  $I_e = 0.5$ ,  $I_s = 1.5$ ,  $\alpha = 1.5$ . Two clusters of bursting are seen with increasing number of spikes with coupling strength,  $\epsilon = 5.0$  (upper left row),  $\epsilon = 8.0$  (middle left row),  $\epsilon = 9.7$  (lower left row).

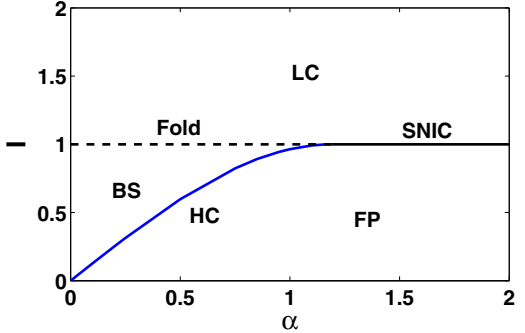


FIG. 3. (Color online) Phase diagram in  $I - \alpha$  space. Limit cycle (LC) zone is separated from the bistability (BS) regime via the fold bifurcation (dashed line). Stable fixed point (FP) is separated from the LC region by the solid SNIC line. Homoclinic (HC) bifurcation line separates BS and FP regimes.

where  $\theta$  is the quantum mechanical phase difference between the macroscopic wave functions on either side of the junction,  $v = \dot{\theta}$  is the node voltage of the junction,  $\alpha = [h/2\pi eIR^2C]^{1/2}$  is the damping parameter,  $h$  is the Planck's constant,  $e$  is the electronic charge, and  $I$  is a constant bias current;  $R$  and  $C$  are the junction resistance and capacitance, respectively. It has an equilibrium solution,  $\sin\theta = I_0$ , in a cylindrical space. The stability of the equilibrium is obtained from the  $f'(\theta^*) = \cos\theta^* = (1 - I_0^2)^{1/2}$ , where  $f' = df/d\theta$  at equilibrium  $\theta = \theta^*$ . For  $I_0 < 1.0$ , the model clearly has two equilibrium points, a node for  $f'(\theta^*) < 0$ , and a saddle for  $f'(\theta^*) > 0$ . The junction starts firing or oscillating above a current threshold  $I_0 = 1.0$ . For  $\alpha < 1.19$ , a fold bifurcation is recorded at  $I_0 = 1.0$  as shown in Fig. 3. In addition there is a bistable region for  $I_0 < 1.0$  and  $\alpha < 1.19$ . For a choice of  $\alpha > 1.19$ , the equilibrium points coalesce at  $I_0 = 1.0$  via SNIC bifurcation [1,3] and finally vanish for  $I_0 > 1.0$  when a limit cycle appears. We focus here on the SNIC regime of  $\alpha > 1.19$ , where the stable equilibrium is separated from the oscillatory regime by the bifurcation line ( $I_0 = 1.0$ ). In this parameter region, the junction behaves like a Type-I excitability neuron [11], in the sense, that the device starts firing or oscillating above the threshold bias current ( $I_0 = 1.0$ ) and the time period of oscillation increases monotonically [9] with the bias current. We select the parameters of the RCSJs of the network from both sides (higher and lower  $I$ ) of the SNIC line (Fig. 3); no intrinsic slow variable exists there in an uncoupled state of the junctions.

## III. NETWORK OF JUNCTIONS

We consider a population of  $N$  globally coupled RCSJ units in which  $l$  number of oscillators are in excitable mode ( $I_e < 1.0$ ) and  $(N - l)$  units are self-oscillatory ( $I_s > 1.0$ ). The network thus consists of two sub-populations and its dynamics is described by two sets of equations, where the coupling is established via the junction node voltage [8],

$$\ddot{\theta}_e + \alpha\dot{\theta}_e + \sin\theta_e = I_e + \frac{\epsilon}{N} \sum_{j=1}^N (\dot{\theta}_j - \dot{\theta}_e), \quad (2)$$

$$\ddot{\theta}_s + \alpha\dot{\theta}_s + \sin\theta_s = I_s + \frac{\epsilon}{N} \sum_{j=1}^N (\dot{\theta}_j - \dot{\theta}_s), \quad (3)$$

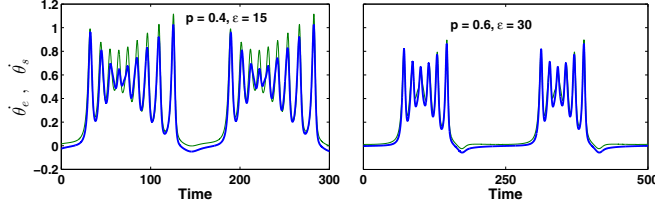


FIG. 4. (Color online) Time series of  $\dot{\theta}_e$  ( $e = 1 \dots l$ ) and  $\dot{\theta}_s$  ( $s = l+1 \dots 100$ ) for all the nodes in a network of size  $N = 100$  for two sets of values of ( $p = 0.4, \epsilon = 15$ ) and ( $p = 0.6, \epsilon = 30$ ) shown as thick blue (black) and green (grey) lines. Other parameters are  $I_e = 0.5, I_s = 1.5, \alpha = 1.5$ .

and  $e = 1, 2, \dots, l$  and  $s = l+1, l+2, \dots, N$  denote the original excitable and self-oscillatory units, respectively.

We choose  $\alpha = 1.5$  for all the junctions to restrict our studies to the SNIC regime. The current bias to the excitable and oscillatory units are chosen as  $I_e = 0.5$  and  $I_s = 1.25$ , respectively, from both sides of the SNIC line (Fig. 3).

For numerical simulations, we consider a network of size  $N = 100$  with an equal number of self-oscillatory and excitable units  $l = 50$ ,  $p = \frac{l}{N} = 0.5$ . Figure 2 reveals a train of bursting oscillation for all the units in the network with increasing coupling strength from the upper to the lower left panels. For a critical coupling and above, the whole population splits into two clusters as seen from the time-series plot of all the oscillators ( $\dot{\theta}_e$ ,  $e = 1, \dots, 50$  and  $\dot{\theta}_s$ ,  $s = 51, \dots, 100$ ) in each panel. In fact, the firing starts with single spiking dynamics (not shown here) above a critical coupling which appears in two distinct clusters. With increasing coupling, one spike after another is added to form the train of bursts (left panels). The number of spikes could be even larger for a further increase of the coupling strength as shown later in the text when we are able to recognize the parabolic nature of the bursting. The bursting in two sub-populations follows each other in time. We mention that the clustering into two sub-populations is a general feature of the junction network since a similar clustering is also found for other values of  $p$ . In support, we present two more examples of the same network size  $N = 100$  but with different ( $p = 0.6, \epsilon = 15$ ) and ( $p = 0.4, \epsilon = 30$ ) values as shown in Fig. 4. It shows the time series of  $\dot{\theta}_e$ ,  $e = 1, \dots, l$  and  $\dot{\theta}_s$ ,  $s = l+1, \dots, 100$  that confirms clustering and parabolic bursting in both sub-populations for two other choices of  $p = 0.4$  ( $l = 40$ ) and  $0.6$  ( $l = 60$ ).

#### IV. REDUCED NETWORK MODEL AND MECHANISM OF BURSTING

Figure 2 (right panels) describes spatio-temporal pattern of all the nodes ( $e = 1, \dots, 50, s = 51, \dots, 100$ ) which further confirms the formation of two clusters. This allows a reduction [20,29] of the large network into subgroups confined to two manifolds,  $\theta_1 = \theta_2 = \dots = \theta_l$  representing the original excitable units and  $\theta_{l+1} = \theta_{l+2} = \dots = \theta_N$  representing the original self-oscillatory units when we represent the network by two oscillators,

$$\ddot{\Theta}_e + \alpha_e \dot{\Theta}_e + \sin \Theta_e = I_e + \epsilon(1-p)(\dot{\Theta}_s - \dot{\Theta}_e), \quad (4)$$

$$\ddot{\Theta}_s + \alpha_s \dot{\Theta}_s + \sin \Theta_s = I_s + \epsilon p(\dot{\Theta}_e - \dot{\Theta}_s), \quad (5)$$

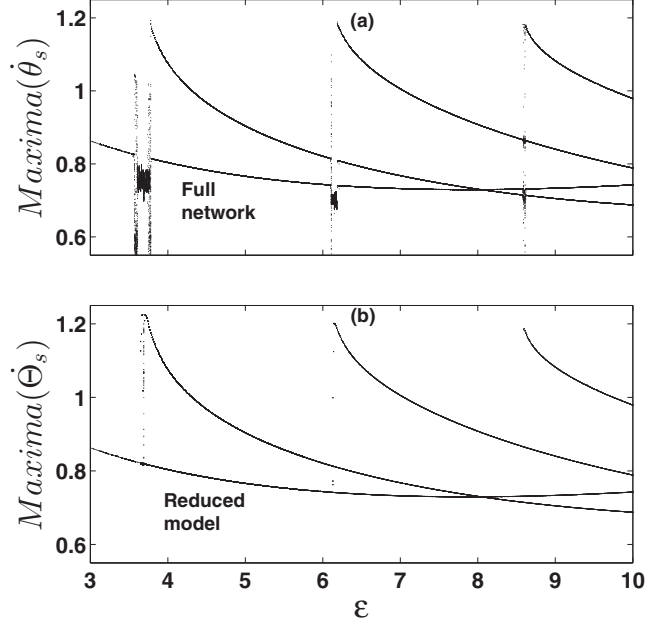


FIG. 5. Bifurcation diagram (maxima of the spikes in the bursts) of one Josephson junction in the network. One unit is arbitrarily chosen from the original oscillatory population ( $51, \dots, 100$ ) and the maxima of  $\dot{\theta}_s$  is plotted as shown in (a), and a corresponding bifurcation diagram from the reduced model is plotted in (b).  $I_e = 0.5, I_s = 1.5, \alpha = 1.5$ .

where  $p$  denotes the fraction of excitable junctions in the whole population and,  $\Theta_s$  and  $\Theta_e$  represent the phase dynamics of the two subgroups of junctions. The details of the stability of equilibrium points of simple two-coupled junctions (oscillatory and the excitable units) are reported elsewhere [28]. We verify here the numerical results of the whole population with the reduced model of two coupled junctions.

Figure 5 presents the bifurcation diagrams (maxima of the spikes in the bursts) of the dynamics of any one unit arbitrarily chosen from the whole network and its reduced model Eqs. (4) and (5) as well. Maxima of  $\dot{\theta}_s$  of one junction node (say,  $s = 1$ ) is plotted with coupling strength ( $\epsilon$ ) in the upper panel that represents a self-oscillatory unit ( $s$ ) of the whole network. For increasing coupling strength, it shows an addition of one spike after another in the regions of periodic bursting. The period-adding regimes (addition of spikes) are intercepted by complex bursting windows. The maxima of  $\dot{\Theta}_s$  of the reduced model is shown in the lower panel and the bifurcation diagram is in good agreement with the upper panel. The windows of complex dynamics are also found to be matching, however, we do not focus here on this complex bursting. The reduced model thereby perfectly represents the dynamics of the whole network. The dynamics represents any of the nodes of the network although one junction is chosen arbitrarily.

The nature of bursting is parabolic [11,14] as shown in Fig. 6. Left panel shows the time series of a single burst; a larger coupling strength is considered here, when the number of spikes is reasonably large. In the right panel, the inter-spike interval is plotted for successive spikes in the burst which shows a parabolic nature. The oscillation starts via SNIC

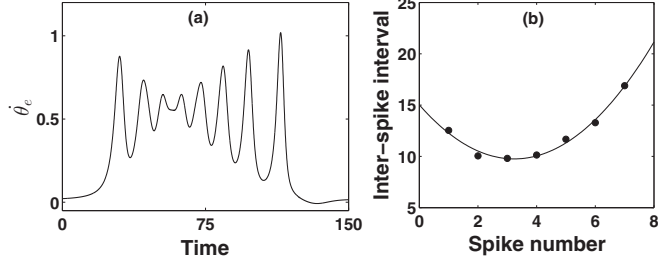


FIG. 6. Parabolic bursting in the network of Josephson junctions. Single burst in the left panel, inter-spike interval shows the parabolic nature in the right panel.  $p = 0.5$ ,  $\epsilon = 20$ ,  $I_e = 0.5$ ,  $I_s = 1.5$ ,  $\alpha = 1.5$ .

bifurcation and stops via SNIC bifurcation and the process repeats.

The presence of excitable junction units induces a slow dynamics in the network that controls the firing (oscillation) and resting (steady) states which is elaborated in Fig. 7. The upper panel demonstrates the parabolic bursting in a 3D plane of  $\dot{\Theta}_e$ ,  $\dot{\Theta}_s$ ,  $\Theta_s$  where a zero plane is drawn in gray (cyan). A part of the trajectory (in a box) goes below the zero plane which is enlarged in the lower panel. We make an observation here that the excitable and the oscillatory units behave like isolated units when the excitable units arrive at the zero plane. The ensemble of excitable units and oscillatory units are reduced to two isolated junctions. The excitable unit tries to return to the steady state and to maintain its isolated dynamics with a node and a saddle that influences the slow-fast bursting of the oscillatory junction. The location of the saddle with its eigen-directions and the node of the uncoupled excitable junction are denoted by open and solid circles, respectively. The trajectory of the bursting, after a few fast spikings, arrives near the zero plane in the gray (cyan) line when it moves towards the saddle guided by the stable manifold of the excitable unit. Effectively,

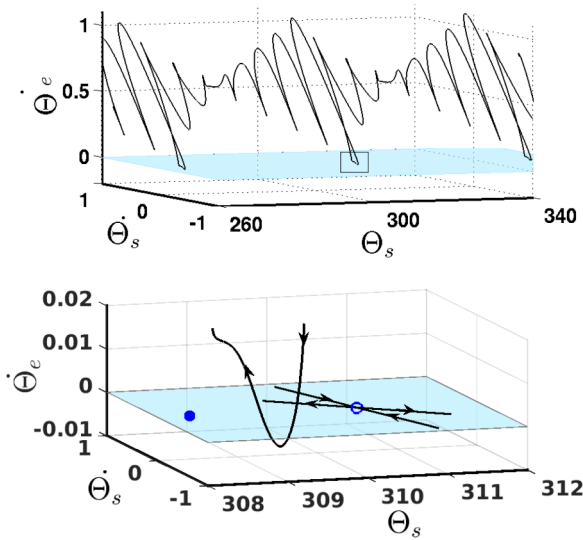


FIG. 7. (Color online) Parabolic bursting of the Josephson junctions. Upper panel shows the bursting in a 3D plane of  $\dot{\Theta}_e$ ,  $\dot{\Theta}_s$ ,  $\Theta_s$ . Lower panel shows an enlarged picture of a part (in a box) of the upper panel.  $p = 0.5$ ,  $\epsilon = 20$ ,  $I_e = 0.5$ ,  $I_s = 1.5$ ,  $\alpha = 1.5$ .

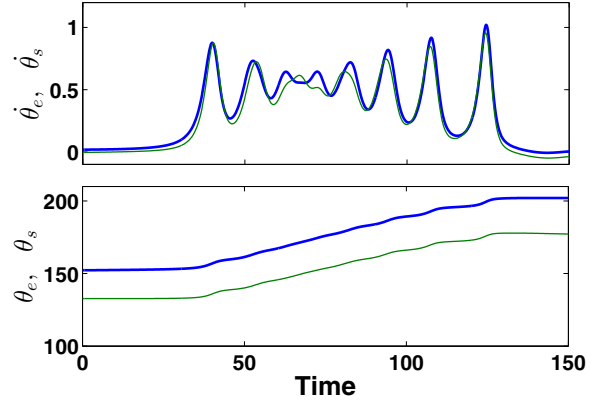


FIG. 8. (Color online) Time series of the voltage variable  $\dot{\theta}_{e,s}$  and phase variable  $\theta_{e,s}$  of all the oscillatory and excitable junction units of the network:  $N = 100$ ,  $I_e = 0.5$ ,  $I_s = 1.5$ ,  $\alpha = 1.5$ .

the trajectory becomes slow when it approaches the saddle point, and after coming sufficiently close to it, moves away by the influence of the unstable eigenvector. The process repeats to generate a train of periodic bursting.

Macroscopically, two sub-populations, excitable and oscillatory, work in a push-pull action: excitable junctions are trying to push the network towards the steady state, while the oscillatory junctions are trying to pull out of the steady state. In this competition, both sub-populations (say, first) oscillate and try to follow each other but lag behind (upper panel of Fig. 2 and left panel of Fig. 8) at the start of oscillation. After a few spikes, they appear at the same time at the end of the burst when the trajectories of both the sub-populations move towards the steady state in the saddle direction. The excitable system actually first crosses the zero line (upper panel in Fig. 2 and left panel of Fig. 8) and loses its influence on the oscillatory units which then start recovering its oscillation and simultaneously pull up the excitable junctions to oscillation. The whole process repeats to generate the train of periodic bursting. The phase dynamics grows during the spiking and remains constant during its slow motion near the steady state (lower panel in Fig. 8).

## V. NETWORK OF MORRIS-LECAR SYSTEM

We investigate the Morris-Lecar model [27] next to construct a network of mixed populations of self-oscillatory and excitable dynamical units. It was considered earlier [21] to show a region of global oscillations where we find a dominant bursting dynamics. The globally coupled network of the ML model is described by

$$\begin{aligned} C\dot{V}_i &= g_L(-V_i - V_L) - g_{Ca}M_{ss}(V_i - V_{Ca}) \\ &\quad - g_KW(V_i + V_K) + \phi(0.2 - V_i) + \frac{k}{N} \sum_{j=1}^N (V_j - V_i), \end{aligned} \quad (6)$$

$$\dot{W}_i = \lambda(V_i)(W_{ss} - W_i), \quad (7)$$

$$M_{ss}(V) = 0.5(1 + \tanh[\frac{V - V_1}{V_2}]); \quad W_{ss}(V) = 0.5(1 + \tanh[\frac{V - V_3}{V_4}]); \quad \text{and} \quad \lambda = \lambda_0(1 + \cosh[\frac{V - V_3}{V_4}]). \quad g_L = 0.5, g_{Ca} = 1,$$

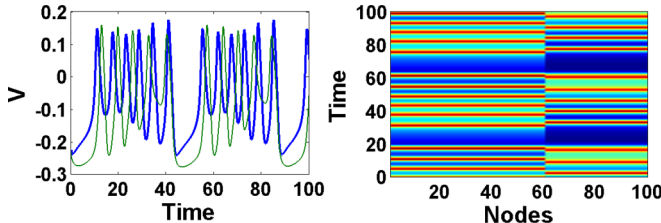


FIG. 9. (Color online) Bursting in a network of 100 Morris-Lecar oscillators with  $p = 0.6$  and  $k = 0.423$ . The thick blue (black) and solid green curves (grey) in the left panel respectively represent the time series of the variable  $V$  for the excitable and oscillatory units. The right panel shows the corresponding space time plot.

$g_K = 2$  are leakage constants,  $V_L = 0.4$ ,  $V_{Ca} = 1$ ,  $V_K = 0.7$ ,  $\lambda_0 = 0.33$ , and  $V_1 = -0.01$ ,  $V_2 = 0.15$ ,  $V_3 = 0.1$ ,  $V_4 = 0.145$ , and  $C = 1.0$  is the membrane capacitance. We mention that we use a global population of  $N = 100$  neurons of which 60 nodes are oscillatory ( $\phi_o = 0.12$ ) and 40 nodes are excitable ( $\phi_e = 0.035$ ).

A linear diffusive coupling is used via the  $V_i$ -variable. The bursting dynamics with two clusters of self-oscillatory and excitable units is clearly revealed in Fig. 9 for a coupling constant,  $k = 0.423$ , however, note that it is not restricted to this coupling strength only. This confirms that the bursting is one of the important dynamical features in the global oscillation regime of a mixed population of the Morris-Lecar system.

## VI. CONCLUSION

We investigated the collective dynamics of a globally coupled network of Josephson junctions basically using the RCSJ model. The network consisted of a mixed population of oscillatory and excitable junctions. We found, in a broad parameter regime of the junction parameter, especially, in the region of SNIC bifurcation and a range of coupling strength, a kind of parabolic bursting in all the nodes of the network. We produced numerical evidence of the phenomenon using a network of  $N = 100$  oscillators. For our chosen coupling strength, the network splits into two clusters when they start spiking. We were then able to reduce the system into a two-oscillator model. Results of the reduced model were found perfectly matching with the numerical results of the whole network. Furthermore, we increased the coupling strength when the clustering was maintained, additionally, one spike

after another arrived to form a bursting dynamics which we explained with bifurcation diagrams of the whole network and its reduced model. We considered examples of three different percentages of excitable units and reproduce the bursting dynamics in all three examples. The bursting is always of parabolic type in the selected parameter regime of the superconducting device where the dynamics is governed by the SNIC bifurcation. It is concluded that the presence of a sub-population of excitable units induces a slow dynamics that is responsible for the bursting dynamics in the network. We explained the mechanism of bursting as a fall out of two competitive sub-populations: a push-pull effect between the excitable and oscillatory units. The excitable units tried to push down the oscillation towards a stable state while the reverse is true for the self-oscillatory units. In the milieu, the bursting as a train of fast spiking periodically interrupted by a slow motion emerges. The bursting dynamics was also found in a network of mixed population of the Morris-Lecar system. The bursting, therefore, seemed to be a generic feature of a mixed population of such dynamical units and independent of the size of the network. A mixed population of oscillatory and excitable units, in general, was investigated earlier by others [20,21], in order to find the existence of global oscillation, if any, besides partial oscillation and oscillation death. It is important to know, in the context of pacemaker cells in the heart or suprachiasmatic cells in the brain, how they sustain global oscillation in a situation of progressive cell death. A region of global oscillation in parameter space was definitely found where the pacemaker cells sustain their activity. However, the particular nature of the oscillation was not focused in the earlier works. Our results, in that sense, provided additional information about the network dynamics of a mixed population of globally coupled oscillators where bursting is found to be one of the important dynamical features in the global oscillation regime. We confirmed emergence of the bursting dynamics using two dynamical models, the superconducting Josephson junction and the Morris-Lecar system.

## ACKNOWLEDGMENTS

The authors thank Baruch Barzel for interesting comments and suggestions and, also acknowledge support a short visit by the MPI-PKS, Dresden. S.K.D. acknowledges funding by the CSIR (India) under the Emeritus Scientist Scheme. P.P. acknowledges support by NIT Durgapur (India) under the Research Initiation Grant Scheme.

- 
- [1] M. Levi, F. C. Hoppensteadt, and W. L. Miranker, *Q. Appl. Math.* **37**, 167 (1978).
  - [2] F. M. A. Salam and S. Shankar Sastry, *IEEE Trans. Circuit Syst. II* **32**, 784 (1985).
  - [3] S. H. Strogatz, *Nonlinear Dynamics and Chaos* (Westview Press, Cambridge, MA, 1994).
  - [4] A. B. Cawthorne, C. B. Whan, and C. J. Lobb, *J. Appl. Phys.* **84**, 1126 (1998).
  - [5] K. Wiesenfeld, P. Colet, and S. H. Strogatz, *Phys. Rev. E* **57**, 1563 (1998); *Phys. Rev. Lett.* **76**, 404 (1996).
  - [6] S. K. Dana, D. C. Sengupta, and K. Edoh, *IEEE Trans. Circuits Syst. I* **48**, 950 (2001).
  - [7] E. Kurt and M. Canturk, *Physica D* **238**, 2229 (2009).
  - [8] V. Vlasov and Arkady Pikovsky, *Phys. Rev. E* **88**, 022908 (2013).
  - [9] S. K. Dana, D. C. Sengupta, and C.-K. Hu, *IEEE Trans. Circuits Syst. I* **53**, 1031 (2006); S. K. Dana, P. K. Roy, D. C. Sengupta, G. Sethia, and A. Sen, *IEE Proc. Cir. Systs. Devices* **153**, 453 (2006).
  - [10] J. Borresen and S. Lynch, *PLoS ONE* **7**, e48498 (2012).

- [11] E. M. Izhikevich, *Int. J. Bifur. Chaos* **10**, 1171 (2000); A. Sherman and J. Rinzel, *Proc. Natl. Acad. Sci. USA* **89**, 2471 (1992).
- [12] P. Crotty, D. Schult, and K. Segall, *Phys. Rev. E* **82**, 011914 (2010).
- [13] C. Baesens and R. S. MacKay, *Nonlinearity* **26**, 3043 (2013).
- [14] G. B. Ermentrout and N. Kopell, *SIAM J. Appl. Math.* **46**, 233 (1986); N. Kopell and G. B. Ermentrout, *Math. Biosci.* **78**, 265 (1986).
- [15] J. Rinzel, *Proceedings of the International Congress of Mathematicians* (Berkeley, California, USA, 1986), p. 1578.
- [16] R. M. Rose and J. L. Hindmarsh, *Proc. R. Soc. London B* **237**, 267 (1989).
- [17] S. Chakraborty and S. K. Dana, *Chaos* **20**, 023107 (2010); S. K. Dana and P. K. Roy, *Int. J. Bifur. Chaos* **17**, 3437 (2007).
- [18] J. Pfeiffer, M. Schuster, A. A. Abdumalikov, Jr., and A. V. Ustinov, *Phys. Rev. Lett.* **96**, 034103 (2006); A. B. Cawthorne, P. Barbara, S. V. Shitov, C. J. Lobb, K. Wiesenfeld, and A. Zangwill, *Phys. Rev. B* **60**, 7575 (1999).
- [19] S. Watanabe and S. H. Strogatz, *Phys. Rev. Lett.* **70**, 2391 (1993); *Physica D: Nonlinear Phenomena* **74**, 197 (1994).
- [20] H. Daido and K. Nakanishi, *Phys. Rev. Lett.* **96**, 054101 (2006).
- [21] D. Pazo and E. Montbrio, *Phys. Rev. E* **73**, 055202(R) (2006).
- [22] G. V. Osipov, O. I. Kanakov, C.-K. Chan, J. Kurths, S. K. Dana, L. S. Averyanova, and V. S. Petrov, in *Complex Dynamics in Physiological Systems: From Heart to Brain, Understanding Complex Systems series*, edited by S. K. Dana *et al.* (Springer, Berlin, 2009).
- [23] R. Singh, J. Xu, N. G. Garnier, A. Pumir, and S. Sinha, *Phys. Rev. Lett.* **108**, 068102 (2012).
- [24] T. B. Luke, E. Barreto, and P. So, *Neur. Comput.* **25**, 3207 (2013).
- [25] J. Jalife, *J. Physiol.* **356**, 221 (1984); D. C. Michaels, E. P. Matyas, and J. Jalife, *Cir. Res.* **58**, 706 (1986).
- [26] A. Kalsbeek, F. Kreier, E. Fliers, H. P. Sauerwein, J. A. Romijn, and R. M. Buijs, *Endocrinology* **148**, 5635 (2007).
- [27] C. Morris and H. Lecar, *Biophys. J.* **35**, 194 (1981); B. S. Gutkin and G. Bard Ermentrout, *Neural Comput.* **10**, 1047 (1998); K. Tsumoto, H. Kitajima, T. Yoshinaga, K. Aihara, and H. Kawakami, *Neurocomputing* **69**, 293 (2006).
- [28] T. Hongray, J. Balakrishnan, and S. K. Dana (unpublished).
- [29] M. Nandan, C. R. Hens, P. Pal, and S. K. Dana, *Chaos* **24**, 043103 (2014).